Crystallographic Effects During Radiative Melting of Semitransparent Materials

B. W. Webb* and R. Viskanta†
Purdue University, West Lafayette, Indiana

Experiments have been performed to illustrate crystallographic effects during radiative melting of unconfined vertical layers of semitransparent material. Radiative melting of a polycrystalline paraffin was performed and the instantaneous layer weight and transmittance were measured using a cantilever beam technique and thermopile radiation detector, respectively. The effects of radiative flux, initial solid subcooling, spectral distribution of the irradiation, and crystal structure of the solid as determined qualitatively by the sample solidification rate were studied. Experimental results show conclusively the dominant influence of crystallographic effects in the form of multiple internal scattering of radiation during the melting process. A theoretical model is formulated to predict the melting rate of the material. Radiation transfer is treated by solving the one-dimensional radiative transfer equation for an absorbing-scattering medium using the discrete ordinates method. Melting rate and global layer reflectance as predicted by the model agree well with experimental data. Parametric studies conducted with the model illustrate the sensitivity of the melting behavior to such variables as incident radiative flux, initial layer opacity (material extinction coefficient), and scattering asymmetry factor.

Nomenclature

A_s = global layer absorptance
c = solid specific heat
f = solid volume fraction
F_s = local radiative flux
F^0 = radiative flux incident on layer
Fo = Fourier number, $\alpha t/L^2$
g = phase function asymmetry factor
Δh_f = latent heat of fusion
I = radiation intensity
k = solid thermal conductivity
L = initial solid layer thickness
m = instantaneous solid layer mass
m_0 = initial solid layer mass
p = scattering phase function
R_s = global layer reflectance
Ste^* = modified Stefan number, $F^0cL/k\Delta h_f$
t = time
T_f = fusion temperature
T_s = global layer transmittance
x = coordinate direction
α = thermal diffusivity, $k/\rho c$
β = extinction coefficient, $\sigma + \kappa$
κ = absorption coefficient
λ = wavelength
μ = direction cosine
ρ = density of phase change material
ρ^* = reflectivity of air-phase change material interface
σ = scattering coefficient
τ = optical depth
τ_L = optical thickness, $\int_0^L \beta(x)dx$
ω = single scattering albedo, $\sigma/(\sigma + \kappa)$

Received Oct. 22, 1986; revision received March 9, 1987.

*Research Assistant. Presently with the Dept. of Mechanical Engineering, Brigham Young University, Provo, Utah.

†W.F.M. Goss Distinguished Professor of Engineering, Heat Transfer Laboratory, School of Mechanical Engineering. Associate Fellow AIAA.

Introduction

RADIATION-induced melting of semitransparent materials is of interest to a wide variety of important technologies. Melting of glass batch and other materials processing, growth of pure crystals from melts and solutions, ablative cooling of re-entry vehicles, elimination of ice and frost layers from buildings and the aircraft fuselage are just a few of the applications where greater understanding of the fundamental transport processes is needed. Little research has been done, from a fundamental viewpoint, on the radiative transport and subsequent melting of the materials.

The effect of crystal structure and orientation in the solid phase of a material can be an important factor when considering radiative melting of a semitransparent phase change medium. The presence of randomly oriented grains in the solid interior can result in multiple internal scattering of thermal radiation at the grain boundaries. Depending on the opacity of the sample, the result can be radically different melting characteristics than those found in single-crystalline substances. Previous investigators have shown the importance of crystallographic effects during radiative melting of ice. Seki et al.[1-3] studied radiative melting of clear and cloudy ice layers in horizontal and vertical configurations. Lamps of two different spectral distributions were used in the study, corresponding to radiation source temperatures of approximately 800 and 3200 K. Two different crystal structures in the ice samples were studied corresponding to rapid and slow initial solidification. The experimental results showed the strong influence of radiation transport in the melting process.

Gilpin et al.[4] also studied experimentally and theoretically the radiation-driven melting of a vertical unconfined ice layer. It was shown that the extent of crystal formation and the trapping of air bubbles during the initial freezing of water strongly affects the internal scattering in the ice. A theoretical model was formulated for determining the radiative transport in the ice layer. The two-flux approximation was used in the radiative transfer equation, and the scattering phase function used in the model was measured experimentally. Predictions were made only for the temperature rise of the solid due to sensible heating; no melting was simulated.

A purely theoretical treatment of the effects of internal scattering on melting and solidification of a semi-infinite semitrans-

parent material was presented by Oruma et al.[5] Model results showed that anisotropic scattering significantly affects the rate of propagation of the melting (solidification) front. Backward scattering was shown to retard melting, while forward scattering enhanced it. No comparison was made with experimental data.

This study was undertaken to investigate more conclusively such issues as the sample preparation procedure and resulting crystal structure, the spectral distribution and magnitude of the incident radiative flux, and the initial solid subcooling. These parameters were isolated systematically, and their influence on the melting rate was studied for radiative melting of a pure, polycrystalline substance. Experiments were performed and a model was formulated for the study of radiative melting of a semitransparent material.

Experiments

Test Apparatus

A schematic of the test apparatus used for studying the radiative melting of an unconfined vertical layer of semitransparent materials is shown in Fig. 1. A 5.5 cm diam cylindrical wafer of semitransparent material (research grade, 99% pure n-octadecane, $T_f = 27.4$°C) was suspended at the end of an aluminum cantilever beam 39.4 cm long with a 6.4 mm square cross section. The cantilever was attached rigidly to a tubular steel mounting post. Strain gages mounted on the beam at the upper and lower surfaces next to the mounting post were connected to a bridge amplifier, whose output was fed to a digital voltmeter. The cantilever beam assembly was calibrated by suspending known weights at the end and tabulating the corresponding strain gage voltage. The resulting calibration proved to be linear to within 0.02% with a calibration constant of 0.615 mV/g. The calibration constant was then used to determine the instantaneous weight of the melting wafer suspended at the end during the experiments. The magnitude of the incident radiative flux was measured with a thermopile (Eppley, No. 4967) connected to a digital voltmeter. This thermopile was also used to estimate the instantaneous radiant energy transmitted through the melting sample.

Two different radiation sources were used in the study. The radiation flux from the two sources had quite different spectral distributions. An array of solar simulation lamps (Philips, 13117) were used to produce a spectral distribution approximating emission from a blackbody at 5800 K, and a 250 W tungsten filament photographic lamp mounted in a parabolic reflector was used to simulate emission from a blackbody at 3200 K. Both lamp systems provided uniform radiation over the 5.5 cm diam paraffin wafers to within 8%. The thermopile used to determine the incident radiation was also calibrated by the manufacturer for accurate flux measurement for both spectral distributions.

A constant temperature bath was also used to solidify the paraffin samples and to achieve the desired initial solid temperature prior to each experiment.

Experimental Procedure

Each experiment began with the preparation of the test material. Since the crystal structure was expected to have an effect on the radiant energy transport and absorption in the solid, the manner of sample preparation was carefully documented. The paraffin was first thoroughly degasified by subjecting it to a cycle of melting and solidification under vacuum. This was done to eliminate unwanted bubbles in the solid, which would have doubtlessly affected the energy transport and overall melting process. After degasification the liquid paraffin was siphoned into a brass mold of cylindrical cross section with 5.7 cm inside diam. The mold was then partially immersed in a constant temperature bath preset to a desired solidification temperature. An incandescent lamp was used to heat the top layer during solidification such that the freezing process would proceed from the bottom of the mold upwards, eliminating the formation of voids and a crust on the top surface.

Two different crystal structures and/or grain orientations were achieved by varying the solidification rate during the sample preparation. During one sample preparation process, the liquid paraffin was rapidly solidified by maintaining the constant temperature bath in which the brass mold was immersed at a temperature 20°C below the fusion temperature of the phase change material. In the second preparation procedure, the constant temperature bath was maintained 5°C below the fusion temperature. After total solidification, the cylindrical paraffin blocks were removed from the mold by slight heating and stored in air-tight containers until used.

Sixteen hours prior to each experiment the temperature of the laboratory was set to a few tenths of a degree below the fusion temperature of the paraffin. This minimized the heat transfer by convection and radiation between the melting solid and the ambient surroundings. The cylindrical samples were cut into wafers approximately 2.3 cm thick. The wafers were then placed in air-tight bags and immersed in the constant temperature bath preset at the desired initial solid temperature. The sixteen hours of equilibration ensured that the initial solid temperature was equal to that of the constant temperature bath, which was 0.2 to 0.3°C below the fusion temperature for most of the experiments.

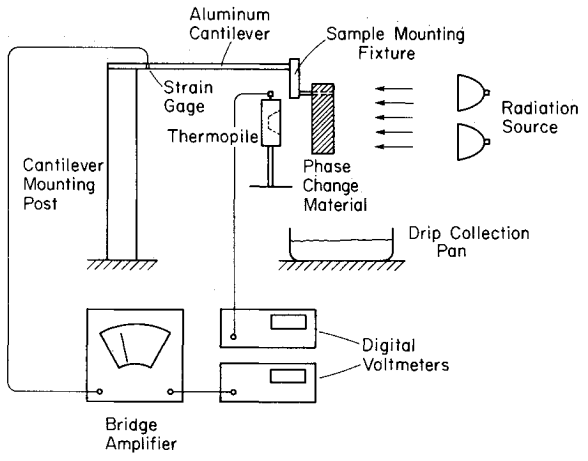

Fig. 1 Schematic of experimental apparatus.

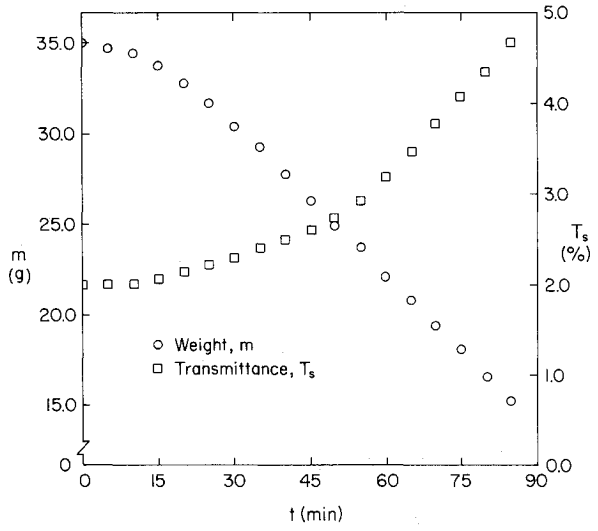

Fig. 2 Timewise variation of sample weight and transmittance for $F^0 = 1440$ W/m², 5800 K radiation source, slowly solidified samples, negligible subcooling.

The radiation source was positioned at the desired location, and the radiation flux was measured at several locations corresponding to different depths in the solid. The average of these measurements was used in quantifying the incident radiation flux. A reference radiation flux was also measured at the back of the wafer mounting location for use in the transmittance measurements. The solid wafers were then mounted on a fixture at the end of the cantilever beam. The experiment was begun by reading and recording the initial weight of the solid sample. Power was then supplied to the radiation source. Readings were recorded from the two digital voltmeters corresponding to instantaneous weight and transmittance measurements at preselected times during the experiment.

Experimental Results

The experimentally measured instantaneous wafer weight and transmittance is shown as a function of time in Fig. 2 for a typical experiment with a slowly solidified sample. Both variables show a monotonic variation with time as expected; the wafer weight decreases as melting proceeds, whereas the transmittance increases as the wafer thins. An initial transient period usually lasted 10–15% of the total melting time. The solid paraffin wafer begins each experiment with a smooth surface; after a short period of time, a rough melting front develops as shown in Fig. 3. Shown in Figs. 3a and 3b are photographs of the solid/liquid interface morphology taken after approximately 80 min of melting for initially slowly and rapidly solidified samples, respectively. The melting front appears to be slightly more nonuniform for the slow solidification case, with larger grains protruding from the surface. Other photographs contrasting the melt front for the two different preparation procedures (not shown) also revealed that the rapidly solidified sample was somewhat more "milky" than the slowly solidified sample. These observations seem to suggest that the grains in the solid crystal structure are smaller for the rapid solidification preparation procedure. This is consistent with traditional materials solidification theory.[6]

The initial transient in the melting process is believed to be due to the time required for the development of this rough melting surface, after which the nearly linear melting behavior seen in Fig. 2 prevails. The jagged melting surface illustrates the local effect of crystal structure on the scattering and/or absorption of thermal radiation on the melting process. The grain boundaries present sites of local scattering of radiation. The resulting solid/liquid interface is radically different from the smooth morphology characteristic of melting from a heated surface.[7–10] A rough melting surface was also observed for radiative melting of cloudy (rapidly solidified) ice by Seki et al.[3] and was attributed to a tendency toward internal radiative melting of the ice sample.

After the initial melting transient, the experiments were characterized by quasisteady melting during which the melting rate was very nearly constant. The constant melting rate is not surprising since the radiation flux incident on the sample is constant. The melting rate was quantified for each experiment during the linear melting regime by curve-fitting the data using least-squares regression. In all experiments, the correlation coefficient for the fit was higher than 0.999, indicating that the sample weight/time relationship in the quasisteady regime was virtually linear. Scattering in the interior of the solid paraffin was evident during each experiment by a "glowing" of the melting solid. The brilliance of the glow was most intense just inside the surface of irradiation incidence; attenuation of the glow was clearly visible toward the back of the sample.

As discussed previously, solid samples of different internal crystal structures and/or orientations were prepared by solidifying the degasified paraffin either rapidly or slowly. Care was taken to insure that the two different samples were the same size initially, and that the incident flux was exactly the same for the two experiments. Figure 4 illustrates the melting behavior for the rapidly and slowly solidified samples under otherwise identical experimental conditions. The duration of the initial

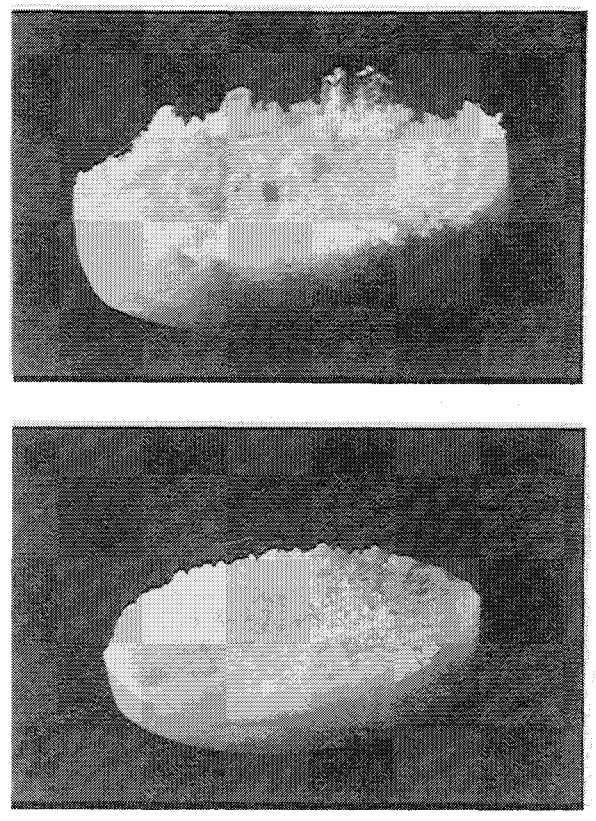

Fig. 3 Photograph of magnified crystal structure illustrating the melting surface morphology for $F^0 = 1440$ W/m², 5800 K radiation source, negligible subcooling: a) slowly solidified sample, b) rapidly solidified sample.

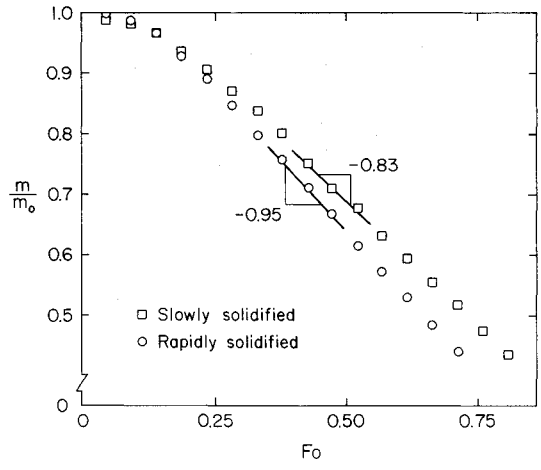

Fig. 4 Effect of sample preparation procedure on melting for $F^0 = 1440$ W/m², 5800 K radiation source.

melting transient is about the same for the two samples. There is a clear difference in the melting rate for the rapidly vs slowly solidified samples, as indicated in the figure. The dimensionless melting rate, $-\mathrm{d}(m/m_0)/\mathrm{d}Fo$, as given by the least-squares regression for the rapidly solidified sample, is 15% higher than that for the slowly solidified sample. This is significant in light of the fact that all other experimental conditions were the same. Gilpin et al.[4] have shown that internal scattering in the solid can actually increase the internal heating, resulting in more rapid melting. The results of this study then suggest that multiple internal scattering of thermal radiation is more preva-

lent in the rapidly solidified solid than in the slowly solidified sample.

Figure 5 shows melting characteristics of the solid paraffin for the two radiation sources simulating emission from blackbodies at 3200 and 5800 K for the same nominal incident radiation flux. Surprisingly, the source whose emission is concentrated more strongly in the infrared part of the spectrum (3200 K source) produces more than double the melting rate of the higher temperature source. Recall that the fraction of blackbody emission beyond 1 μm for the 3200 and 5800 K radiation sources is 62 and 28%, respectively.[11] As seen in Fig. 6, the absorption characteristics for n-octadecane[12] reveal that the material is much more strongly absorbing in the infrared part of the spectrum; the spectral absorption coefficient increases several orders of magnitude from the visible to the near infrared part of the spectrum. Accordingly, absorption is expected to dominate over internal scattering for wavelengths beyond 1 μm. The higher melting rate seen for the lower temperature radiation source can therefore be explained by the greater fraction of radiant energy in the infrared part of the spectrum.

It is instructive at this point to introduce a theoretical limiting case melting rate. If one assumes that the sample is opaque ($\tau_L \to \infty$), initially at its fusion temperature, and further that the reflection at the surface of incident radiation is negligible, the dimensionless melting rate of the solid can be shown to be

$$-\frac{d(m/m_o)}{dFo} = Ste^* \tag{1}$$

where the modified Stefan number is defined in the Nomenclature. The limiting case assumption of a perfectly opaque solid is not far from the physical system studied here, since the opacity of the samples based on an approximate extinction coefficient of $\beta = 300\ m^{-1}$ (see Fig. 6) is of order six or seven. Any deviations from the theoretical limiting value of the dimensionless melting rate are primarily the result of radiant energy scattered out of the system because the reflectance of the rough, front surface is at most only a few percent. Deviations due to transmission through the sample are small since the transmittance was never higher than 5%. The experimentally correlated melting rates for the 3200 and 5800 K radiation sources as shown in Fig. 5 were 2.05 and 0.95, respectively. The corresponding theoretical limiting melting rates as given by Eq. (1) were 2.09 and 2.15, respectively. The melting rate for the 3200 K source is only 2% lower than the theoretical limit, whereas the corresponding rate for the 5800 K source is 56% lower. The 3200 K source shows better agreement with the limiting value because of the reduced influence of internal scattering of radiation in the solid. As was stated before, the spectral distribution of emission from the 3200 K lamp is more concentrated in the wavelength region where absorption dominates over scattering.

Figure 7 shows the melting process for radiative melting of the n-octadecane wafers with initial solid subcooling of 10.4 and 0.4 deg. C below the fusion temperature. The initial melting transient appears to be of longer duration for the subcooled solid. Seemingly, it takes longer for the subcooled solid to attain the melting front morphology found in the quasisteady melting regime. Additionally, the correlated melting rate for the subcooled solid is 15% lower than that for the negligible subcooling case. This is due to the radiant energy required to sensibly heat the subcooled solid to its fusion temperature.

Analysis of Radiative Melting

A methodology has been formulated for predicting the radiative transfer in an unconfined layer of absorbing-scattering semitransparent material and the subsequent melting. The experimental observations presented in the foregoing suggest that a model based on multiple internal scattering of radiation and melting is appropriate. A known spectral radiation flux F^0 is incident on a vertical layer of unconfined phase change mate-

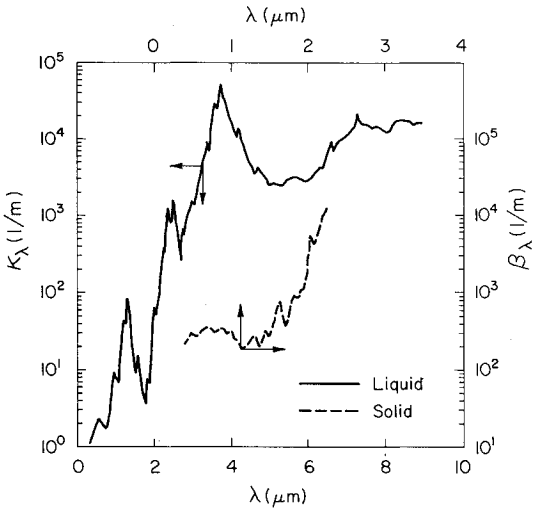

Fig. 6 Spectral absorption (extinction) coefficient of n-octadecane.[12]

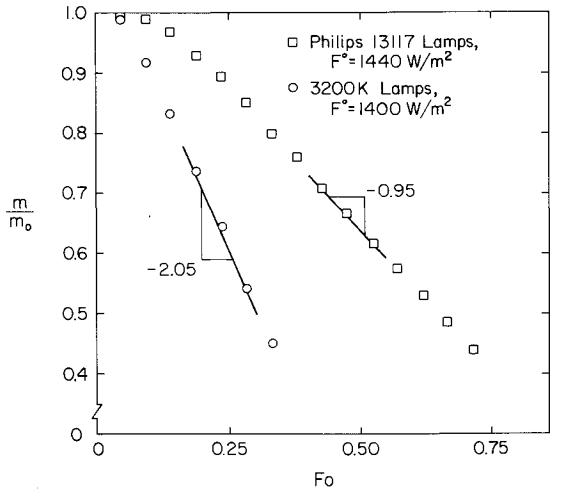

Fig. 5 Timewise variation of solid weight for the 3200 K and 5800 K radiation sources, $F^0 = 1400$ and 1440 W/m², respectively, rapidly solidified samples.

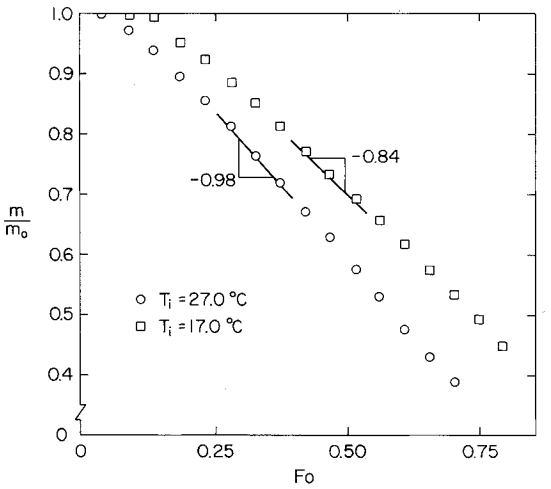

Fig. 7 Effect of initial solid subcooling on the melting rate for $F^0 = 1900$ W/m², 5800 K radiation source, slowly solidified samples.

rial. The radiation flux penetrates the medium where internal scattering and absorption occur. Melting occurs by forming a porous matrix of solid and liquid. The following assumptions are invoked in the analysis. The radiation transfer is one-dimensional and azimuthally symmetric with homogeneous radiative properties. The phase change material is capable of absorbing and scattering thermal radiation, but temperatures are low enough that emission can be neglected. The material is at its fusion temperature. (Previous investigations have shown the effects of scattering on semitransparent materials in the absence of phase change[13–15]; hence, this analysis is confined to the case where absorption of radiation results only in change of phase rather than sensible heat rise of the solid.) Finally, it is assumed that as melting occurs, the melt flows out of the porous matrix, and the liquid drips from the suspended wafer.

Governing Equations

Under the framework of the foregoing assumptions the partial differential equation governing the local melting of the phase change material may be stated as

$$\rho \Delta h_f \frac{\partial f_s}{\partial t} = \frac{\partial F}{\partial x} \tag{2}$$

where f_s is the volume fraction of the solid phase in the porous matrix. The radiation field has been assumed to be one-dimensional. Note that Eq. (2) requires only an initial condition on the solid volume fraction distribution $f_s(0, x) = 1$. Boundary conditions will, however, be necessary for the calculation of the radiative flux divergence. Note that it is the local absorption of the radiant energy as given by the flux divergence distribution that gives rise to local melting and subsequent change in the solid volume fraction.

Under the assumptions outlined previously, the quasisteady radiative transfer equation is[16]

$$\mu \frac{\mathrm{d}I(\tau, \mu)}{\mathrm{d}\tau} = -I(\tau, \mu) + \frac{\omega}{2} \int_{-1}^{+1} p(\mu', \mu) I(\tau, \mu') \mathrm{d}\mu' \tag{3}$$

Although not explicitly indicated, the terms in Eq. (3) must be treated on a spectral basis. The optical depth is defined as

$$\tau = \int_0^x \beta(x) \mathrm{d}x \tag{4}$$

The dimensionless spectral radiative flux may be determined by integrating the intensity over all directions

$$\bar{F}(\tau) = 2\pi \int_{-1}^{+1} I(\tau, \mu) \frac{\mu \mathrm{d}\mu}{F^0} \tag{5}$$

The dimensionless radiative flux divergence may also be calculated as

$$\bar{H}(\tau) = -\beta \frac{\partial \bar{F}(\tau)}{\partial \tau} \tag{6}$$

Boundary conditions for the radiative transfer equation must be specified in order for the problem to be well-posed. Since the back boundary is transmitting, it is equivalent to a black boundary with none of the radiation that reaches this boundary being either reflected or scattered back into the medium. The back boundary is simply specified then as being radiatively black. Rather than attempt to model the reflection characteristics of the jagged morphology at the surface of incident radiation, reflection there is neglected. This may be justified by the fact that for a material with an index of refraction of $n = 1.43$, normal reflection of collimated radiation is very small (approximately 3%). However, the sensitivity of the predicted results of this assumption will be assessed later.

The scattering phase function distribution must be defined as part of the radiation transfer problem. The phase function employed here is expanded in a series of Legendre polynomials about the scattering angle using the series form

$$p(\xi) = \sum_{k=0}^{N} (2k + 1) g^k P_k(\cos\xi) \tag{7}$$

where $N = 150$ has been shown to accurately represent both isotropic and anisotropic scattering,[14] and was therefore used in this study.

Method of Solution

Due to the complexity of the radiation absorption in the absorbing-scattering material, it is unlikely that a closed-form solution exists. Recourse was therefore taken to a numerical solution. The energy equation governing local melting, Eq. (2) was discretized by integrating around a typical control volume and applying an explicit scheme in time. After the calculation of the local solid fraction at the new time step the total solid remaining was calculated by integrating

$$\frac{m}{m_0} = \int_0^1 f_s \mathrm{d}\left(\frac{x}{L}\right) \tag{8}$$

The solution of Eq. (2) assumes knowledge of the radiative flux divergence. This comes from integration of the radiative transfer equation. The radiation field was determined by the method of discrete ordinates. This approximation divides the radiation field into any number of M discrete streams, providing for very high angular resolution of the radiation field. The scattering phase function is expanded in a series of Legendre polynomials as given by Eq. (7). The integral of Eq. (3) is then replaced by a Lobatto quadrature formula. Appropriate boundary conditions are applied at the two extremes of the domain. The result is a system of M coupled, linear, nonhomogeneous differential equations of the form

$$\begin{aligned} \mu_i \frac{\mathrm{d}I_i(\tau, \mu_i)}{\mathrm{d}\tau} &= -I_i(\tau, \mu_i) \\ &+ \frac{\omega}{2} \sum_{i=1}^{M} I_i(\tau, \mu_i) a_i \sum_{k=0}^{N} \bar{w}_k P_k(\mu_i) P_k(\mu_k) \\ &+ \frac{\omega}{2} [1 - \rho^*(\mu_c^*)] \frac{\mu_c^*}{\mu_c} F_c^0 \exp\left(\frac{-\tau}{\mu_c}\right) \\ &\times \sum_{k=0}^{N} \bar{w}_k P_k(\mu_i) P_k(\mu_c) \quad 1 \le i \le M \end{aligned} \tag{9}$$

Note that under the assumption of zero reflectivity at the boundary of incidence, $\rho^* = 0$. The method employed for solution of Eq. (9) is given in detail by Houf and Incropera.[14] While it has been reported that the discrete ordinates technique can become numerically ill-conditioned if the number of ordinates, M, is taken to be greater than 25, it was found that for the combination of high scattering and large optical depth used in this study a value of M larger than 10 resulted in a numerically ill-conditioned system of equations. Therefore, 10 was the maximum number of ordinates used in the computations. Numerical experiments with fewer ordinates, however, showed only a 7% change in the global reflectance of the absorbing-scattering layer with 8 vs 10 ordinates. After calculations to find the optimum time step and grid size for accurate results, time increments of $\Delta t = 7.5$ s and $\Delta x/L = 100$ were selected. Computations with smaller time increments showed no change in the melting rate in two decimal places.

It should be mentioned that the melting front retracts from the lamp array as the wafer melts. This was simulated by allowing the incident radiation to impinge on the first control volume with solid volume fraction greater than 5%. As melting proceeded and the solid continued to retract, the radiation field was recomputed for the layer of decreasing opacity. The ap-

proximate 2–3% temporal variation in F^0 as the melting front retracts was handled by using the average flux measured experimentally over the sample depth. The incident radiative flux was also assumed to be entirely collimated at normal incidence.

A two-band model was used to treat the spectral dependence of radiation properties. As seen in Fig. 6, solid n-octadecane is effectively opaque beyond a wavelength of 2.0 μm.[12] Accordingly, a semitransparent band was assumed below this critical wavelength, and all thermal radiation in wavelengths above 2.0 μm was assumed to be deposited at the surface of the melting front. Additionally, it was assumed, for lack of better data, that the absorption coefficients of the solid and liquid phases of the paraffin were equal, as is characteristic of single-crystalline substances. The single-scattering albedo is estimated to be $\omega = 0.95$; and as seen from the very large albedo, the sample is expected to be highly scattering.

Comparison of Predictions with Experiments

The predicted variation of the sample weight with time is compared to the experimental data for $F^0 = 1440$ and 2680 W/m^2 in Fig. 8. The cylindrical wafer depth L was chosen arbitrarily as the characteristic length in the dimensionless time and modified Stefan number. The inputs to the model in simulating these experiments were $\beta = 300\ \mathrm{m}^{-1}$, $g = 0$ (isotropic scattering), and $\omega = 0.95$. No information is provided in Ref. 12 about sample preparation before measuring the extinction coefficient of solid n-octadecane. Isotropic scattering was assumed without knowledge of the angular distribution of the scattering phase function. The assumption of isotropic scattering will be verified by parametrically varying the value of the phase function asymmetry factor in a section to follow. The initial layer opacity was estimated to be about $\tau_L = \beta L \cong 7$. The solid symbols indicate the experimental data used to initialize the simulation. As seen in the figure, there is virtually no discrepancy between model predictions and experimental data for the $F^0 = 1440$ W/m^2 case (for $\beta = 300\ \mathrm{m}^{-1}$). The discrepancy is only slightly greater for the higher flux case. The approximate 10% difference is, however, within the experimental uncertainty in magnitude of the incident flux, thermophysical properties, etc. The agreement is quite good in light of the major assumptions made in the model formulation.

Also shown in Fig. 8 is the model sensitivity ot uncertainties in the value of extinction coefficient. Simulations were carried out for values of the extinction coefficient 20% higher and lower, respectively, than the base case value. The results show that the model is moderately sensitive to the value used, but that the estimated base case value is a reasonable one.

One parameter of great interest is the timewise variation of the global reflectance of the sample. Although this was not measured directly it can be determined in the following way. A radiant energy balance on the layer of phase change material at any given time yields

$$A_s + T_s + R_s = 1 \tag{10}$$

where A_s, R_s, and T_s are the layer absorptance, transmittance, and reflectance, respectively. The transmittance of the layer was measured experimentally. The absorptance of the layer can be calculated from the melting rate as the ratio of energy absorbed as latent heat and resulting in a change of mass to the total radiant energy incident on the layer:

$$A_s = \frac{\Delta h_f}{F^0 A}\frac{\mathrm{d}m}{\mathrm{d}t} \tag{11}$$

where A is the sample area exposed to the incident radiation flux. The total radiant energy reflected from the sample can then be calculated by rearranging Eq. (10). Note that in the quasisteady melting regime, the melting rate is constant and, hence, the absorptance of the layer is invariant with time. Fig-

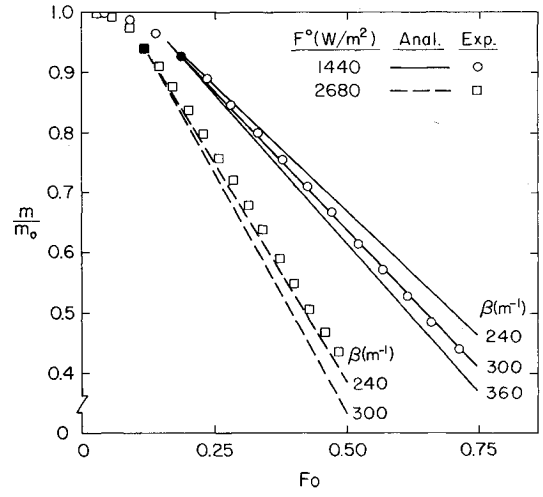

Fig. 8 Comparison of predicted instantaneous weight with experimental data for $F^0 = 1440$ and 2680 W/m^2, 5800 K radiation source, rapidly solidified samples, $L = 2.22$ cm, $g = 0$ (isotropic scattering), $\omega = 0.95$.

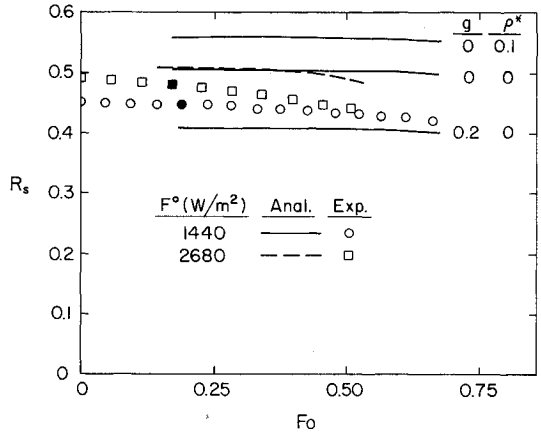

Fig. 9 Comparison of predicted and experimental global layer reflectance for $F^0 = 1440$ and 2680 W/m^2, 5800 K radiation source, rapidly solidified samples, $\tau_L = 6.66$, $\omega = 0.95$.

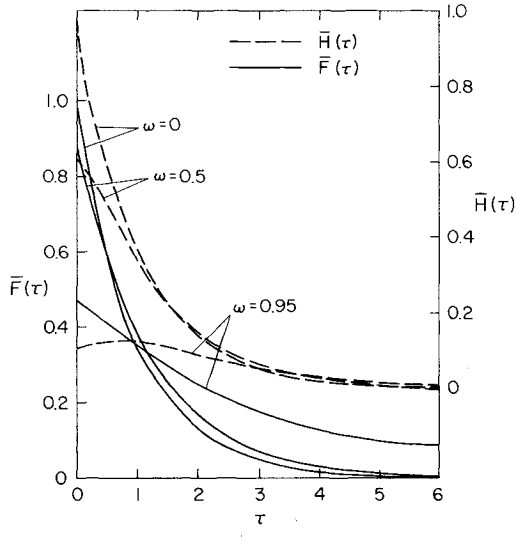

Fig. 10 Predicted profiles of normalized radiative flux and flux divergence for $F^0 = 1440$ W/m^2, $\tau_L = 6.0$, $\omega = 0.95$, $g = 0$.

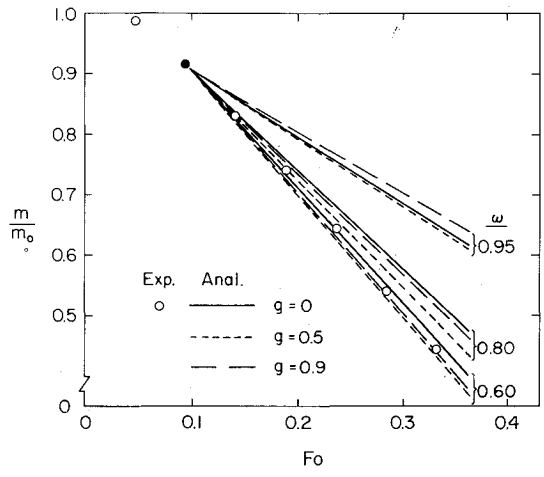

Fig. 11 Comparison of predicted instantaneous weight with experimental data for $F^0 = 1400$ W/m², 3200 K radiation source, rapidly solidified sample, $\tau_L = 6.66$.

ure 9 compares the predicted timewise variation of the global layer reflectance with that determined experimentally for the same conditions of Fig. 8. The trend for the reflectance is a monotonic decrease with time, however slight. This trend is seen for both experimental data and model predictions. The slight decrease is the result of the thinning of the layer and the resulting decrease in its ability to scatter thermal radiation back out of the system. Global reflectance predictions agree quite well with the experimental data. The maximum absolute deviation in R_s between prediction and data is about 0.08 for $g = 0$ and $\rho^* = 0$. Results of additional calculations designed to investigate model sensitivity to the neglect of reflection from the rough melting front show (not unexpectedly) that neglecting surface reflection tends to underpredict the reflectance of the layer. It is also observed that a more strongly forward scattering material ($g = 0.2$) predicts a lower global reflectance than the isotropic scattering simulation ($g = 0$). This, too, is as expected since radiant energy is scattered deeper into the melting solid for a more highly forward scattering material. The results show that the assumptions made concerning reflection losses from the front surface and the angular distribution of the scattering phase function model reasonably well the physical phenomena.

The predicted normalized flux divergence (volumetric heating rate) and the normalized flux are shown plotted as a function of the optical depth in Fig. 10. The input data used to generate the figure are $F^0 = 1400$ W/m², $\tau_L = 6.0$, $g = 0$, and the purely collimated radiation at zero incidence for $\omega = 0$, 0.5, and 0.95. The predicted global layer reflectance was 0, 0.12, and 0.53 for the three values of the single scattering albedo, respectively. The results show clearly that internal scattering of radiation for higher albedoes reduces the radiative flux divergence primarily in the first half of the layer depth. Much of the radiant energy incident on the layer for $\omega = 0.95$ is lost from the system in the form of back-scattered radiation. Consequently, the melting rate for such strongly scattering material will be lower than that for a material where absorption is expected to be the more dominant contribution to extinction of radiation. Notice that for $\omega = 0.95$ the radiative flux divergence is not a maximum at the surface but at some distance from the interface. Since the collimated flux undergoes almost a simple exponential decay, the existence of this maximum cannot be attributed to the absorption of collimated radiation. Instead, it is due to radiation which has been scattered from the collimated beam and is eventually absorbed by the material due to multiple internal scattering. This local maximum in the local heating rate has been predicted previously[13] for isotropic scattering ($g = 0$) and strongly forward scattering ($g = 0.8$) materials. The transmittance of the layer is simply the net normalized flux at the back of the layer, $\tau = 6$. Note also that the magnitude of the normalized radiative flux at the surface is not unity, but rather $1 - R_s$ for this case where the surface reflection has been neglected.

Figure 11 shows the results of predictions for the experiment with the 3200 K radiation source, where the value of the phase function asymmetry factor is varied between 0 and 0.9 for three values of the single scattering albedo. The simulation with single scattering albedo of 0.95 and $g = 0$ showed a dramatically lower melting rate than that of the experimental data. The reason for the discrepancy is the spectral content of the irradiation. Notice that the simulations carried out for lower values of ω approach more closely the experimental melting data. The radiant energy of the incandescent lamp used to simulate the 3200 K source is concentrated much more in the infrared part of the spectrum than the 5800 K source lamps. The absorption coefficient of the paraffin is also dramatically higher in the infrared. Consequently, the single scattering albedo is expected to be lower for the spectrum of emission of the 3200 K source. There is also some question as to the appropriateness of the assumption that the absorption coefficient of the liquid and the solid are the same. One may conclude that absorption dominates over scattering in the infrared part of the spectrum. Also underlined is the need for accurate (absorption and scattering) radiative property data in analyzing this type of system.

The scattering phase function has only a minor effect on the predicted melting rate as seen in Fig. 11. It may also be observed that for a given value of the albedo there is a maximum melting rate which occurs for some value of the asymmetry factor between 0 and 0.9. The value of g corresponding to the maximum melting rate is seen to be a function of the single scattering albedo.

Conclusions

Experiments have been performed to investigate the influence of crystal structure and the resulting internal scattering of radiation on the melting of an unconfined layer of semitransparent phase change material. The experimental results show that the internal structure and orientation of the grain boundaries strongly influence the radiation transport and subsequent melting. An increase in the magnitude of the incident radiant flux has the effect of increasing the melting rate. Radiation sources with higher spectral energy content in regions where the absorption coefficient is high melt more rapidly than materials exposed to radiation sources concentrated in the visible where scattering appears to be dominant. Initial solid subcooling retards the melting process, since a portion of the incident radiant energy is used in sensibly heating the solid to its fusion temperature.

A methodology has been presented for predicting the radiation transfer in the absorbing-scattering solid and the melting which results from local volumetric radiative heating. The radiative transfer equation is solved by the method of discrete ordinates with the option of including anisotropic scattering. The radiative flux divergence thus calculated is used as source term in the energy equation governing local melting of the phase change material. Model predictions agree well with experimental data for the 5800 K radiation source; the predicted timewise variations of the instantaneous weight and global layer reflectance deviated little from the experimental data. However, predictions made for the 3200 K radiation source showed significant discrepancy with measured data. Computations with lower albedo compared much better with data. It is concluded that accurate spectral absorption and scattering property data are needed to accurately predict the radiative transport and subsequent melting for radiation sources whose spectral distribution is concentrated in the infrared where absorption dominates over scattering.

The authors have made no attempt to account for variation in radiative properties at the solid-liquid interface in the analysis. The focus of this study was the interaction of the radiation

field with the internal crystal structure in the solid. More work is clearly needed in modeling the detailed radiative interaction in the interior of the solid and at the nonuniform melting front. For this purpose more reliable spectral radiative property data are needed, including crystallographic effects which are influenced by solid sample preparation.

Acknowledgments

This work was supported in part by the National Science Foundation under Grant No. MEA-8313573. One of the authors (B. W. W.) gratefully acknowledges the financial assistance of his graduate studies by an Eastman Kodak Company Graduate Fellowship.

References

[1]Seki, N., Sugawara, M., and Fukusako, S., "Radiative Melting of a Horizontal Clear Ice Layer," *Warme-und Stoffubertragung*, Vol. 11, 1978, pp. 207–216.

[2]Seki, N., Sugawara, M., and Fukusako, S., "Back-Melting of a Horizontal Cloudy Ice Layer with Radiative Heating," *ASME Journal of Heat Transfer*, Vol. 101, 1979, pp. 90–95.

[3]Seki, N., Sugawara, M., and Fukusako, S., "Radiative Melting of Ice Layer Adhering to a Vertical Surface," *Warme-und Stoffubertragung*, Vol. 12, 1979, pp. 137–144.

[4]Gilpin, R. R., Robertson, R. B., and Singh, B., "Radiative Heating in Ice," "*ASME Journal of Heat Transfer*, Vol. 99, 1977, pp. 227–232.

[5]Oruma, F. O., Ozisik, M. N., and Boles, M. A., "Effects of Anisotropic Scattering on Melting and Solidification of a Semi-Infinite, Semi-Transparent Medium," *International Journal of Heat and Mass Transfer*, Vol. 28, 1985, pp. 441–449.

[6]Flemings, M. C., *Solidification Processing*, McGraw-Hill, New York, 1974.

[7]Ho, C. J. and Viskanta, R., "Heat Transfer During Melting from an Isothermal Vertical Wall," *ASME Journal of Heat Transfer*, Vol. 106, 1984, pp. 12–19.

[8]Benard, C., Gobin, D., and Martinez, F., "Melting in Rectangular Enclosures: Experiments and Numerical Simulations," *ASME Journal of Heat Transfer*, Vol. 107, 1985, pp. 794–803.

[9]Okada, M., "Melting from a Vertical Plate Between Insulated Top and Bottom Surfaces," in *Proceedings ASME/JSME Thermal Engineering Joint Conference*, Vol. 1, ASME, New York, 1983, pp. 281–288.

[10]Bareiss, M. and Beer, H., "Experimental Investigation of Melting Heat Transfer with Regard to Different Geometric Arrangements," *International Communications in Heat and Mass Transfer*, Vol. 11, 1984, pp. 323–333.

[11]Siegel, R. and Howell, J. R., *Thermal Radiation Heat Transfer*, Second Edition, Hemisphere, Washington, D.C., 1981.

[12]Diaz, L., "Radiation-Induced Melting of a Semitransparent Phase-Change Material," Ph.D. Thesis, Purdue University, West Lafayette, Indiana, 1983.

[13]Bergman, T. L., Houf, W. G., and Incropera, F. P., "Effect of Single Scatter Phase Function Distribution on Radiative Transfer in Absorbing-Scattering Liquids," *International Journal of Heat and Mass Transfer*, Vol. 26, 1983, pp. 101–107.

[14]Houf, W. G. and Incropera, F. P., "An Assessment of Techniques for Predicting Radiation Transfer in Aqueous Media," *Journal of Quantitative Spectroscopy and Radiative Transfer*, Vol. 23, 1980, pp. 101–115.

[15]Armaly, B. F. and Lam, T. T., "Influence of Refractive Index on Reflectance from a Semi-Infinite Absorbing-Scattering Medium with Collimated Incident Radiation," *International Journal of Heat and Mass Transfer*, Vol. 18, 1975, pp. 893–899.

[16]Ozisik, M. N., *Radiative Transfer*, Wiley Interscience, New York, 1973.